Revisiting diagenesis on the Ontong-Java plateau: evidence for authigenic crust precipitation in *Globorotalia tumida*

Oscar Branson[1], Elizabeth Read[1], Simon Redfern[1], Christoph Rau[2], and Henry Elderfield[1]

Corresponding author: O. Branson, oscarbranson.work@gmail.com

[1]Department of Earth Sciences, University of Cambridge, Downing St, Cambridge CB2 3EQ, UK

[2]Diamond Light Source Ltd, Diamond House, Harwell Science & Innovation Campus, Didcot, Oxfordshire OX11 0DE, UK

This article has been accepted for publication and undergone full peer review but has not been through the copyediting, typesetting, pagination and proofreading process which may lead to differences between this version and the Version of Record. Please cite this article as doi: 10.1002/2014PA002759

Abstract

The calcite tests of foraminifera lie in marine sediments for thousands to millions of years, before being analysed to generate trace element and isotope palaeoproxy records. These sediments constitute a distinct physio-chemical environment from the conditions in which the tests formed. Storage in sediments can modify the trace element and isotopic content of foraminiferal calcite through diagenetic alteration, which has the potential to confound their palaeoceanographic interpretation. A previous study of *G. tumida* from the Ontong Java Plateau, western equatorial Pacific, found that preferential dissolution of higher-Mg chamber calcite, and the preservation of a low-Mg crust on the tests significantly reduced whole-test Mg/Ca and Sr/Ca [*Brown and Elderfield*, 1996]. Here, we revisit these specimens with a combination of synchrotron X-ray computed tomography (sXCT) and electron probe microanalyses (EPMA) to re-evaluate the nature of their diagenetic alteration. The dissolution of higher-Mg calcite with depth was directly observed in the sXCT data, confirming the inference of the previous study. The sXCT data further reveal a thickening of the chemically and structurally distinct calcite crust with depth. We propose that these crusts have a diagenetic origin, driven by the simultaneous dissolution of high-Mg chamber calcite and precipitation of low-Mg crust from the resulting modified pore-water solution. While the breadth of the study is limited by the nature of the techniques, the observation of both dissolution and re-precipitation of foraminiferal calcite serves

to demonstrate the action of two simultaneous diagenetic alteration processes, with significant impacts on the resulting palaeoproxy signals.

1. Introduction

The trace element and isotopic content of foraminiferal calcite are commonly used as indicators of paleoceanographic conditions. These palaeoproxy records incorporate inherent uncertainties: during life biological calcification processes modulate trace element and isotope incorporation, and after deposition in the sediments diagenetic processes have the potential to alter or overwrite the original composition of the test calcite. Biologically-driven variations in trace element and isotope content are poorly understood, but can be overcome using robust, species-specific calibrations [e.g. *Elderfield et al.*, 2006]. In contrast, diagenesis is poorly constrained, spatially and temporally variable, and much harder to address [e.g. *Schrag et al.*, 1995; *Schrag*, 1999; *Pearson et al.*, 2001].

One of the initial uses of foraminiferal chemistry was to assess the effects of diagenesis on carbonate sediments [*Friedman*, 1964; *Dodd*, 1967], which highlights potential problems for the derivation of palaeo-environmental information from foraminiferal calcite. The term 'diagenesis' encompasses a wide variety of complex processes that bring about changes in a sediment [*Bathurst*, 1975; *Berner*, 1980]. Because of this complexity, the extent of diagenetic overprinting of trace element and isotopic chemistry is hard to constrain [*Frank et al.*, 1999; *Pearson et al.*, 2001], as the nature and extent of alteration depends on the physio-chemical sedimentary environment (which can change through time), and the length of time they have been buried. This introduces a significant source of uncertainty in carbonate-derived palaeoproxies [*Lorens et al.*, 1977; *Savin and Douglas*, 1973].

Four diagenetic processes have the potential to influence the trace element and isotope chemistry of carbonate biominerals: dissolution of original material, precipitation of

new chemically distinct material, adsorption of chemicals onto the mineral surface, and solid diffusion of tracers in to or out of the mineral. These processes can be roughly divided into 'structural' [dissolution/precipitation; *Sexton et al.*, 2006] and 'non-structural' [adsorption/solid diffusion; *Lorens et al.*, 1977; *Savin and Douglas*, 1973] processes. However, these categories are not all-encompassing: for example, neomorphic recrystallisation of biominerals can occur at the nano-scale, replacing the original test structure such that the new material is almost indistinguishable from the old [*Folk*, 1965; *Sexton et al.*, 2006].

Throughout the development and application of carbonate palaeoproxies, attempts have been made to quantify the influence of diagenesis. These attempts have included comprehensive observational investigations [*Berger*, 1970; *Pearson et al.*, 2001; *Sexton et al.*, 2006], chemical models [*Richter and DePaolo*, 1987, 1988; *Richter and Liang*, 1993; *Schrag et al.*, 1995; *Lohmann*, 1995; *Schrag*, 1999], trace element mass balance estimates of dissolution [*Brown and Elderfield*, 1996], and comparative chemical studies of foraminifera deemed to be more- or less-well preserved [*Pearson et al.*, 2001; *Kozdon et al.*, 2013]. Estimates of diagenesis from these studies vary widely between locations and species, ranging from reports of 'pristine' samples preserved in terrigenous deposits [*Pearson et al.*, 2001], to extensively altered specimens from below the lysocline on the Ontong-Java plateau [*Brown and Elderfield*, 1996].

A significant barrier to understanding diagenetic alteration is the disparity between the behaviours of model inorganic calcite, and biomineral carbonates [*Berner and Morse*, 1974; *Honjo and Erez*, 1978; *Baker et al.*, 1982; *Morse and Arvidson*, 2002; *Hales*, 2003; *Morse et al.*, 2007]. Pressure-related thermodynamic effects, the non-linear response of

dissolution kinetics to variations in saturation state, the effect of trace element impurities on dissolution, and the complex architecture of biominerals, where organic components can alter the geometry and availability of dissolution surfaces, all distance the sedimentary dissolution environment from laboratory studies. However, while the complexity of diagenetic processes render a complete systematic understanding of diagenesis unlikely, it is important to characterise the end-members of diagenetic alteration, and understand the vulnerability of samples to different types of alteration in different sedimentary environments. To this end, we have employed high-resolution phase-contrast X-ray computed tomography to quantify the diagenetic alteration of *G. tumida* form the Ontong-Java Plateau.

X-ray computed tomography techniques have been previously applied in in semi-quantitative appraisals of foraminifera dissolution [*Johnstone et al.*, 2010, 2011], and studies of foraminiferal morphology and evolution [*Schmidt et al.*, 2013]. Previously used techniques have either been relatively low resolution [$\sim 7\mu$m in *Johnstone et al.*, 2010, 2011], or focused primarily on phase density imaging [at 1.4μm resolution. *Schmidt et al.*, 2013]. Here, we employ a high-resolution (0.45μm) variation of the technique with high phase contrast sensitivity. This allows us to identify the boundaries between distinct regions of the foraminiferal test, and discriminate between calcite phases that are of similar density but have distinct fabrics, or are separated by a boundary. We couple these measurements with spatially resolved electron microprobe chemical analyses (EPMA) to investigate the trace chemistry of these different calcite regions. Analyses are restricted to well-characterised samples of *Globorotalia tumida* (a sub-thermocline plank-

tic foraminifera) from the Ontong-Java Plateau (OJP), previously analysed by *Brown and Elderfield* [1996].

1.1. Diagenesis on the Ontong-Java Plateau

The Ontong-Java Plateau (OJP) in the western Pacific has been the site of several studies considering the effects of diagenesis [*Lingen and Packham*, 1975; *Berger et al.*, 1982; *Elderfield et al.*, 1982; *Brown and Elderfield*, 1996; *Rosenthal et al.*, 2000; *Mekik and Raterink*, 2008; *McCorkle et al.*, 1995]. Foraminifera from region site suffer from poor preservation [*Shipboard Scientific Party*, 2001], and as such it provides an ideal location at which to investigate an end-member case for early carbonate diagenesis.

Brown and Elderfield [1996] set out to investigate depth-related trends in trace element ratios (M/Ca) seen in planktic foraminifera collected from core top samples from the OJP [*Lorens et al.*, 1977; *Rosenthal and Boyle*, 1993; *Russell*, 1994]. If preservation is perfect, depth-related trends should not appear in core top planktic foraminifera of the same species, which will have lived and calcified at approximately the same time, at the same depth, and in relatively uniform conditions. The existence of these depth-related trends is evidence for the post-depositional modification of foraminiferal chemistry, reported in numerous studies [*Brown and Elderfield*, 1996; *Rosenthal and Boyle*, 1993; *Mekik and Raterink*, 2008; *Regenberg et al.*, 2006, 2014]. While the occurrence of post-depositional modification is uncontroversial, the extent of the alteration, and the processes involved have been the subject of some debate.

In their study of *G. tumida* and *Globigerinoides sacculifer*, *Brown and Elderfield* [1996] conclude that depth-related trends observed in the species are the result of the preferen-

tial dissolution of higher-impurity, and therefore more soluble, calcite. Their conclusion is primarily based on the observation of bimodal calcite composition in *G. tumida*, which is revealed through electron microprobe analyses to have higher Mg in 'primary' chamber calcite, and lower Mg in a fringe of 'keel' calcite. Based on this, and experimental dissolution experiments, they conclude that the primary (higher-impurity) calcite preferentially dissolves below the lysocline, giving rise to the depth-driven changes in Mg content. However, subsequent micro-analytical studies of the dissolution of *Orbulina universa, Globigerinoides ruber* and *Globigerinoides sacculifer* have found no such evidence of the preferential dissolution of higher-impurity regions within the test [*Sadekov et al.*, 2010; *Fehrenbacher and Martin*, 2014], and argue that such dissolution would be insufficient to drive the lysocline-related Mg/Ca trends in these species. Further studies report universal, species independent dissolution rate based on carbonate saturation [*Regenberg et al.*, 2014], while others find that early diagenetic effects are highly species and location specific [*Mekik and Raterink*, 2008; *Johnstone et al.*, 2010]. In essence, the effects of diagenetic alteration on foraminiferal trace elements, the mechanics of these processes, and their relation to laboratory dissolution experiments are poorly understood.

Brown and Elderfield [1996]'s study considered the comparison between primary 'chamber' calcite, and outer 'crust' calcite, which they considered synonymous with the 'keel' calcite of *G. tumida*. According to definitions in the literature (Table 1), this outer enclosing calcite should more appropriately be labelled 'crust', as it is present on the whole test, rather than the outer fringe. With this distinction in mind, we revisit the specimens

of *Brown and Elderfield* [1996] with novel techniques to investigate the subtleties of early diagenesis in *G. tumida*.

2. Methods

G. tumida specimens from the Ontong Java plateau were taken from unused samples prepared by *Brown and Elderfield* [1996]. The internal structure of the specimens was measured using phase-contrast optimised synchrotron X-ray Computed Tomography (sXCT) at the I13 imaging beamline of the Diamond Light Source synchrotron (Rutherford Appleton Laboratory; *Pešić et al.* [2013]; *Rau et al.* [2011, 2007a, b]). Electron microprobe chemical analyses (EPMA) were performed using a Cameca SX100 at the University of Cambridge.

2.1. Synchrotron X-Ray Computed Tomography

The I13 tomography beamline (*Pešić et al.* [2013]) uses highly collimated X-rays to allow the detection of slight changes in the angle of an incident beam [following Snell's law; *Wolf and Krötzsch*, 1995], highlighting differences in refractive indices across material boundaries. The incoming beam is refracted at boundaries in the sample, creating an angular divergence in the transmitted ray, dependent on the magnitude of the phase difference. This angular difference translates to a 'bright' and a 'dark' edge on either side of a phase boundary in the projection image, as transmitted photons are diverted from their original course towards one side of the phase boundary. The allows the instrument to detect phase boundaries that are much finer than its nominal spatial resolution.

2.2. Tomographic Data Collection and Reconstruction

Individual foraminifera were attached to aluminium sample pins using gel super-glue, such that the specimens were suspended tens of microns above the top of the sample pin. Optimum phase contrast for the foraminiferal samples was determined to be at 15 keV (undulator gap 5.26 mm), with a sample-detector distance of 23 mm. Images were collected every 0.1° through a 180° rotation, totalling 1800 projection images, with 1.5 s exposure per image. A 10x optical objective was used to provide a spatial resolution of 0.45 μm per detector pixel. Sets of 20 darkfield (shutter closed) and brightfield images (shutter open, sample out) were taken periodically throughout each scan, and summed to provide bright and darkfield reference images to normalise for inhomogeneities in illumination and detector efficiency, following:

$$Sample_{norm} = \frac{Sample - Darkfield}{Brightfield - Darkfield} \quad (1)$$

Multi-angle stacks of projection images were converted to a 3D data volume using proprietary routines available at the beamline. The reconstruction produces a stack of 2D image slices normal to the rotation axis, every 0.45 μ through the sample.

2.3. Tomographic Data Segmentation

Two data segmentation approaches were applied to the data: slice-based segmentation of single, full-resolution image slices, and 3D segmentation of downsampled 3D data volumes. The former is analogous to the approach used by previous SEM studies, which analyse 2D views of broken test walls, or resin-embedded test cross sections. The latter 3D approach is unique to sXCT, and allows the quantitative assessment of structural modification, which is highly variable throughout the test, and could easily be missed in the single slice view of SEM studies.

Data segmentation labels pixels (or voxels, a pixel in three dimensions) as either 'crust' or 'chamber' calcite (Fig. 2). The slice-based segmentation was performed by hand on a random set of image slices, using FIJI image analysis software [*Schindelin et al.*, 2012].

3D segmentation was performed using the itk-SNAP program [*Yushkevich et al.*, 2006] using the 'adaptive paintbrush tool'. This tool fills a 3D volume of a defined size based on the brightness, and presence of sharp gradients within an initial box - i.e. if the centre of the box was placed on one side of a sharp phase contrast boundary, the selection would not cross that boundary. In areas where the boundary between materials was poorly defined, the boundary was extrapolated manually.

2.4. Electron Microprobe Probe and SEM Analyses

After tomographic analysis, the same samples were mounted in EpoFix© resin, polished to a 3 μm finish and carbon coated. The polished specimens were imaged in a JEOL JSM-S20 SEM, and analysed for trace element chemistry using a Cameca-SX100 electron microprobe.

Individual point measurements of Ca, Mg and Sr were collected using a defocussed beam and a longer count time to increase the signal:noise ratio ($\sim 4\mu$m Θ, at 10 nA and 15 keV, 3 s dwell). Point measurements of Ca, Sr and Mg were calibrated to diopside, celest and olivine (St. Johns), respectively, yielding relative standard deviations of 5% for Mg and Sr. Median detection limits for Ca, Sr and Mg were 1367, 491 and 171 ppm. Approximately 50% of Mg and 10% or Sr measurements were below the limit of detection. For analytical purposes, these values were imputed as half the instrumental detection limit [*Helsel*, 1990],as measurements below the detection limit are still analytically relevant as

'low concentration' end members, even though their precise concentrations cannot be established.

The composition data were non-parametric. Therefore, material compositions were compared using 2-way Kruskal-Wallace H-tests, and depth correlations were assessed using a Pearson correlation coefficient test, both using the scipy.stats package in Python [*Jones et al.*, 2001].

3. Results

3.1. Tomography

Tomograms were collected from a total of 11 specimens from seven depths (Fig. 1) bisecting the lysocline. The number of specimens was limited by the nature of the sXCT technique, but triplicate specimens from the shallowest and deepest locations were analysed to provide an estimate of the reproducibility.

The data show the presence of the characteristic *G. tumida* 'keel' structure, as well as a distinct, blocky calcite crust, particularly on specimens from deep core tops (Fig. 1). As the keel structure is contiguous with the primary 'chamber' calcite, both keel and primary calcite morphotypes are grouped together and labelled 'chamber' calcite, distinct from the enclosing 'crust' calcite (Fig. 2). This schema of 'chamber' and 'crust' calcite types was adopted throughout image analysis, with 'test' referring to the entire structure (including both calcite types).

With increased depth the external sutures (features delineating the chamber boundaries) and porous structure of the chamber wall become less distinct, and are eventually replaced by a coarse, blocky 'crust' (Fig. 1). Internally, gaps appear within the chamber

walls in mid-range depths, and internal structures disappear altogether in the deepest samples. Pristine chamber calcite from shallow depths is structurally complex, with signs of internal laminations, and numerous fine pore structures. The external blocky crust lacks internal laminations, but does occasionally exhibit signs of a porous structure. These structural observations reiterate the results of previous SEM studies of foramifera preservation, which examine either broken foraminiferal tests [*Pearson et al.*, 2001; *Sexton et al.*, 2006], or resin-embedded cross sections [*Kozdon et al.*, 2009, 2011, 2013]. However, our 2D and 3D segmentation data highlight the differences between slice-based techniques, and measuring the entire specimen: 2D segmentation data from multiple slices through individual tests show considerable scatter (Fig. 3), highlighting the heterogeneity of modification throughout the test. This demonstrates that studies seeking to extrapolate from 2D slices to entire tests are sensitive to the position of the cross section. While mean of the 2D data reveals a similar pattern to the 3D data (Fig. 3), it would be possible to find the opposite trend in these specimens, or no trend at all if a only single cross-sectional view of each specimen is available. The 3D data allows the accurate assessment of the abundance of different calcite morphotypes throughout the entire test, overcoming the internal heterogeneity of modification. The 3D segmentation technique is subject to the same subjectivity in determining the location of the test/crust boundary, but excludes the major uncertainty derived from the view location, inherent in 2D data.

In the 3D data, and the mean of the 2D data, the length-normalised crust abundance shows a marked increase with depth, while chamber calcite shows the reverse trend. Fur-

thermore, 3D measurements of length-normalised whole wall thickness also increase with depth, implying a thickening of the test wall.

When considered in terms of % abundance, the proportion of crust calcite increases with depth, and the proportion of chamber calcite decreases with depth, in general agreement with *Brown and Elderfield* [1996]. However, the magnitude of the change, and the absolute % values measured here differ between 20-75% from *Brown and Elderfield* [1996]'s modelled values.

3.2. Chemical Data

Crust calcite has significantly lower Mg/Ca (crust=0.37±0.33, chamber=0.99±1.53, H=74.8, $p < 0.001$, N=381, values reported as median±IQR) and Sr/Ca (crust=1.30±0.37, chamber=1.42±0.42 mmol/mol, H=12.9, $p < 0.001$, N=400) than the test calcite (Fig. 5). Chamber Mg/Ca also displays a much larger range than crust calcite, in-line with the presence of intra-test chemical heterogeneity [*Sadekov et al.*, 2005]. These results agree with those of *Brown and Elderfield* [1996], who found significantly lower Mg and Sr in the 'keel' ('crust', here) calcite, than in the chamber calcite.

Chemical depth transects (Fig. 5) also showed similar trends to *Brown and Elderfield* [1996], with a significant decrease in whole-test Mg/Ca ($R = -0.17 \pm 0.003$, p=0.001, N=381) and Sr/Ca ($R = -0.22 \pm 0.01$, $p < 0.001$, N=381) over the entire core-top depth range. Independent correlation analyses of crust and chamber calcites revealed that these depth-relationships were predominantly driven by reductions in crust trace element content with depth. Both crust Mg/Ca ($R = -0.16 \pm 0.004$, p=0.02, N=214) and Sr/Ca ($R = -0.23 \pm 0.02$, p=0.001, N=214) decreased significantly with depth, while there were

no significant depth relationships in chamber Mg/Ca ($R=0.11 \pm 0.16$, $p=0.16$, $N=167$) or Sr/Ca ($R=-0.10 \pm 0.02$, $p=0.20$, $N=167$).

4. Discussion

4.1. Evidence for Dissolution

In general, our data corroborate the findings of *Brown and Elderfield* [1996]. Both structural and chemical aspects of our data offer support the increased dissolution of primary chamber calcite at depth. Or sXCT data reveal a decrease in absolute (Fig. 3) and relative (Fig. 4) chamber abundance with depth, accompanied by a visible disintegration of both internal and external chamber wall structure (Fig. 1). Our EPMA analyses confirm that Mg/Ca and Sr/Ca are lower in the crust than the chamber calcite, and we observe reductions in Mg/Ca and Sr/Ca content with depth in both whole-test and crust calcite, but not in chamber calcite (Figs. 5). This implies that the removal of higher-impurity chamber calcite is the primary driver of the depth-related reductions in whole-test trace element content (Fig. 5). In combination with *Brown and Elderfield* [1996], our data highlight the potential for the dissolution of higher-impurity calcite to influence palaeo-oceanographic proxy records. However, this trend appears restricted to *G. tumida*, as studies of other species do not find evidence of selective dissolution in other species [*Brown and Elderfield*, 1996; *Sadekov et al.*, 2010; *Fehrenbacher and Martin*, 2014].

In an idealised system, dissolution should be negligible above the calcite lysocline, at ~3400 m [*Berger et al.*, 1982]. This should produce a two-step dissolution pattern, with an inflection at a critical carbonate saturation horizon, where dissolution and chemical modification begin. This pattern has been observed in chemical and structural studies

of numerous foraminifera species [*Regenberg et al.*, 2006; *Johnstone et al.*, 2010; *Regenberg et al.*, 2014]. Our data do not exhibit such a step-change in structural or chemical character (Fig. 3and 4). Rather, our *G. tumida* specimens exhibit linear structural and chemical trends with depth, implying significant alteration in the sediment surface above the lysocline. This super-lysocline modification implies that the test experiences local variations in saturation state.

These variations could either be driven by processes that reduce the local saturation environment, or be attributed to variations in impurity content of the chamber calcite, which raises the effective saturation state for specific parts of the structure, making them more vulnerable to dissolution. Localised processes that could expose the test to undersaturated waters include water-column microbial activity in aggregated particles [*Milliman et al.*, 1999], or microbial activity near the sediment-water interface, which can alter the sediment surface saturation state [*Hales*, 2003]. The effect of these processes may be particularly noticeable at the Ontong Java Plateau, because while the lysocline depth is nominally ∼3400 m, seawater is only fractionally supersaturated with respect to ($CaCO_3$) well above the lysocline [below ∼1600 m *Berger et al.*, 1982]. Alongside these local saturation variations, internal chemical and structural heterogeneity in the chamber calcite will render parts of the test more soluble than others. This solubility difference is evident in our mid-depth sXCT specimens, where preferential dissolution along internal laminations is evident. This preferential intra-wall dissolution pattern has not been observed in laboratory studies [*Brown and Elderfield*, 1996; *Sadekov et al.*, 2010], but re-creating the precise dissolution conditions (particularly pressure and time) of deep sea-floor sediments

in a laboratory is challenging, and previous studies may not have captured the mechanics of dissolution in deep sediments.

While internal chemical variations offer a convenient explanation of super-lysocline dissolution of higher-impurity phases, the differences in composition between high- and low-Mg calcite in a foraminifera are small: ∼10 mmol/mol in the similar species *Globorotalia menardii* [*Sadekov et al.*, 2005]. Assuming similar variations in *G. tumida*, *Brown and Elderfield* [1996] estimate that Mg/Ca variations of this magnitude could raise the effective saturation horizon for higher-Mg calcites by up to ∼300 m, given the saturation profile of waters above the Ontong-Java Plateau. In combination with the numerous processes that can modulate the local saturation environment, and our observation of clear laminar intra-chamber wall dissolution, this suggests that intra-test chemical heterogeneity is sufficient to drive differential chamber dissolution above the lysocline.

The preferential dissolution of intra-test high-Mg calcite is able to account for the depth-related trends in trace element content of *G. tumida*. However, dissolution alone can not fully explain the sXCT and chemical data presented here. Rather, our data support a more complex scenario, involving the near-simultaneous dissolution and reprecipitation of foraminiferal calcite.

4.2. Evidence for Reprecipitation?

Foraminiferal crusts of the type observed in this study have been seen in sediment-trap, plankton-tow and laboratory-grown specimens [*Bé and Lott*, 1964; *Orr*, 1967; *Hemleben*, 1975; *Caron et al.*, 1990]. They are therefore often considered a biogenic feature associated with gametogenesis, or a late life cycle stage of the foraminifera [*Brown and Elderfield*,

1996]. In this were the case, the increase in encrusted foraminifera with depth could be driven by the preferential preservation of specimens with low-Mg crusts over non-encrusted specimens. However, the increase in whole-test wall thickness with depth, the increase in absolute crust abundance with depth, and the changes in crust composition with depth all suggest that the crusts observed on *G. tumida* are in fact a diagenetic feature, created by the simultaneous dissolution and reprecipitation of chamber calcite in the sediments.

Firstly, sXCT analyses revealed an increase in the thickness of the chamber wall (including both crust and chamber calcites) with depth (Fig. 3). If dissolution of higher-Mg calcite were the sole driver of the trace element-depth trends observed in *G. tumida*, the opposite wall thickness trend would be expected. Dissolution is a destructive processes, and should lead to chamber walls being thinned, damaged and fragmented in deeper water with lower carbonate saturation. The sXCT data here reveal the reverse trend, implying a post-depositional alteration of foraminifera that leads to wall thickening.

Secondly, sXCT data reveal that test wall thickening is accompanied by an increase in the absolute (length-normalised) amount of crust calcite, and a decrease in the amount of chamber calcite (Fig. 3). This implies that while chamber calcite dissolves in deeper, less-saturated water, the crust calcite accumulates, over-compensating for the dissolution of test calcite and causing an overall increase in wall thickness.

Together, these sXCT data provide strong structural evidence for the simultaneous dissolution and reprecipitation of *G. tumida* calcite. However, inorganic precipitation experiments reveal that calcites precipitated from seawater-like solutions have orders of magnitude higher Mg/Ca than foramiferal calcite [*de Nooijer et al.*, 2014; *Mucci*, 1987].

Our EPMA data reveal that the *G. tumida* crust calcite has lower Mg/Ca and Sr/Ca than the chamber calcite (Fig. 5). While our data support a biogenic crust origin at face value, this is at odds with the thickening of crust calcite with depth, which implies a diagenetic crust origin. Furthermore, reductions in Mg/Ca and Sr/Ca within the crust and whole-test calcite in deeper samples provide support for an alternative, purely diagenetic mechanism that could produce these low-trace element crusts.

Dissolution of higher-Mg *G. tumida* calcite is clearly prevalent in the carbonate sediments of the Ontong-Java plateau. This dissolution leads to the reduction of whole-test Mg/Ca and Sr/Ca content with depth (Fig. 5). Importantly, these depth-related chemical trends are present in the crust calcite, but not in the chamber calcite. If the crusts were biogenic, we would expect them to form at a similar life stage in similar conditions, and therefore have similar composition; there should be no systematic depth-related trends. The change in crust composition with depth is indicative of a variation in crust precipitation environment. Such a change in precipitation environment could be provided by the simultaneous dissolution of higher-trace-element chamber calcite, and precipitation of trace-element-poor crust calcite from the resulting Ca-enriched fluid [*Kozdon et al.*, 2013; *Pearson and Burgess*, 2008; *Edgar et al.*, 2015]. E.g. in marginally saturated pore-water environments, the dissolution of high-impurity chamber calcite would enrich the surrounding pore fluids in a high-Ca, low Mg fluid (relative to seawater), allowing the re-precipitation of a lower-impurity crust phase, which is supersaturated relative to the pore fluids.

Over time, the crust could precipitate in the sediment, growing slowly from a trace-element deplete fluid that is predominantly made from dissolved primary foraminiferal calcite, with possible additions from the dissolution of other biogenic carbonates [*Kozdon et al.*, 2013],Pearson:2008cq,Edgar:2015gy. However, such a system cannot be considered to be completely isolated from seawater, particularly in coretop samples. The relative contribution of chamber dissolution and seawater to the 'parent' solution of the crust can be estimated, by considering its composition as a mixture between fluids of seawater and chamber composition:

$$M/Ca_{parent} = PM/Ca_{sw} + (1-P)M/Ca_{chamber} \quad (2)$$

where P is the proportion of seawater in the fluid, and ranges between 0 and 1. From this, it is possible to estimate the relative contribution of seawater and dissolved chamber calcite, based on the compositions of seawater and chamber calcite, and the range of published inorganic distribution coefficients (K_D) for Sr [0.02 – 0.32; *Mucci and Morse*, 1983; *Nehrke et al.*, 2007] and Mg [0.01 – 0.03; *Mucci and Morse*, 1983; *Oomori et al.*, 1987; *Mavromatis et al.*, 2013], given:

$$K_D = \frac{M/Ca_{crust}}{M/Ca_{parent}} \quad (3)$$

$$K_D = \frac{M/Ca_{crust}}{PM/Ca_{sw} + (1-P)M/Ca_{chamber}} \quad (4)$$

$$P = \frac{M/Ca_{crust} - K_D M/Ca_{chamber}}{K_D M/Ca_{sw} - K_D M/Ca_{chamber}} \quad (5)$$

Using these inorganically-derived K_D estimates, crust and chamber Mg data suggest that between 0.2 ± 0.2 % and 0.7 ± 0.6% of the parent solution is seawater. Conversely, Sr compositions suggest between 35.7 ± 16.1 % and 860 ± 254% of the parent solution is

seawater (i.e. the pore water has 8.6 time more Sr than seawater). Crust Sr content is also high, relative to previously analysed diagenetic calcites [*Kozdon et al.*, 2013; *Hathorne et al.*, 2003; *Edgar et al.*, 2015].

The inconsistency between the Mg- and Sr-derived seawater contribution estimates could either be taken to suggest that there is an additional process removing Mg in the sediments, that there is a pathway for additional Sr to be incorporated into the crusts during deposition, or that the crusts are not diagenetic in origin. Given the depth-related trends in chemistry, crust thickness, and chamber dissolution, it is unlikely that the crusts are a life feature, as discussed previously. The discrepancy between these seawater contribution estimates therefore serve to offer some insight into the precipitation mechanism at work in the sedimentary environment. The relatively high concentration of Mg in seawater, and the absence of a readily available sedimentary Mg removal process, make the reduction of Mg in coretop pore waters unlikely. Furthermore, the high seawater Mg concentration renders crust Mg/Ca particularly sensitive to seawater contributions, making the lower seawater contribution estimates from Mg likely to be closer to reality than the higher Sr-derived estimates. Additional Sr could be provided by an acantharian celestite ($SrSO_4$) flux [*Hill et al.*, 2012; *de Deckker*, 2004], although given that Sr is not elevated in shallow pore waters on the Ontong Java Plateau [*Fantle and DePaolo*, 2006], this is also unlikely. Finally, it is possible that the apparent discrepancy between Mg and Sr data is the result of using distribution coefficient values from laboratory inorganic precipitation experiments, which that are far removed from the sedimentary environment in which the crust is deposited. Furthermore, the dissolution/reprecipitation reaction likely

occurs at the micron-scale, taking place in boundary layers where broad scale chemical gradients become less important [*Pearson and Burgess*, 2008]. Simultaneous dissolution-reprecipitation reactions at mineral-fluid interfaces at these scales have been observed in silicate minerals, and are a vital aspect of weathering processes [*Ruiz-Agudo et al.*, 2012]. If such surface-specific processes were in effect, reduction in concentration from the foraminiferal calcite could be driven by interface-specific inorganic fractionation factors, which could be far removed from those calculated in more 'ideal' solution-based experiments. It is possible at these scales that Mg and Sr experience very different fractionating drives, given the significant difference in ion size, and their ability to be accommodated in the calcite lattice. This could preferentially exclude Mg from the newly precipitated crystal, and allow Sr to persist.

Based on the radial orientation of the calcite rhombohedra in the crust, the original foraminiferal test must act as a nucleation substrate for the diagenetic crust [*Sexton et al.*, 2006]. This allows the superficial preservation of test features (e.g. pores), owing to the preferential growth of calcite along the *c*-axis, and lends the crust a 'biogenic' porous appearance until the crust becomes so extensive that these features are obscured (as in the deepest specimens analysed here; Fig. 1).

This simultaneous dissolution/reprecipitation scenario offers an explanation of the depth-related thickening of foraminiferal walls, the increase in crust abundance, the decrease in test abundance, and the preservation of external test morphology. It augments the dissolution effect observed by *Brown and Elderfield* [1996] with a second diagenetic process, which has the potential to further alter palaeoproxy signals. In the context of

palaeoproxies, this mechanism would complicate their interpretation by introducing both a trace element concentration offset, determined by fractionation factors of trace elements determined by the local sedimentary physio-chemical environment, and a 'smoothing effect', whereby dissolution of foraminifera in adjacent sediment layers might contribute to crust growth, thus homogenising the sediment record. This latter effect would depend upon the rates of vertical pore fluids diffusion within the sediment column. It is also likely that dissolution of non-foraminiferal carbonate (e.g. from coccolithophores) would contribute to the composition of the pore fluid, and consequently the crust calcite.

While this study is limited in scope by the necessarily small sample size, the sXCT technique offers the ability to directly observe structural changes in the foraminiferal test, and accurately quantify the degree of diagenetic alteration. The ability to examine and quantify structural changes of this nature has been lacking in the field of micropalaeontology. While some considerable progress has been made with 2D studies of embedded or broken foraminifera, our data highlight the heterogeneity of test alteration, which drives a disparity between 2D slice data, and complete 3D analyses.

5. Conclusions

The structural and chemical data presented in this study support *Brown and Elderfield* [1996]'s inference that the preferential dissolution of higher-Mg at depth drives reductions in foraminiferal trace element content, and it reveals an additional process that has the potential to modify carbonate-based palaeoproxies: reprecipitation. The sXCT technique can quantify the abundance of different materials within the volume of the foraminiferal test. We find that the primary test calcite dissolves with depth, while the walls of the test

grow continuously thicker, and the abundance of a coarse calcite crust increases. This suggests concomitant dissolution and reprecipitation in *G. tumida* on the Ontong-Java Plateau. Furthermore, chemical analyses of the calcite crust show a decrease in trace element content with depth. Calculations based on our Mg and Sr data suggest that this system could be either 'closed' or 'open', relative to seawater, although it is possible that localised simultaneous dissolution-reprecipitation environments could develop, which are less sensitive to bulk porewater chemistry. The preliminary findings presented here indicate that simultaneous dissolution/reprecipitation reactions do occur in foraminifera in the sediments, and warrant further investigation to explore the details of the processes, and their importance in modifying palaeoproxy records.

Acknowledgments. The authors would like to acknowledge Aleksey Sadekov, Gerald Langer, India Weidle, Alberto de Fanis, Andrew Bodey, Joan Vila-Comamala and Ulrich Wagner for their help with the project. The work was funded by the Diamond Light Source and by the ERC (2010-NEWLOG ADG-267931 grant to HE). Owing to the large data volumes associated with tomographic reconstructions (tens of GB), raw data are not available online. Data are available from the corresponding author on request (oscarbranson.work@gmail.com).

References

Baker, P. A., J. M. Gieskes, and H. Elderfield (1982), Diagenesis of Carbonates in Deep-Sea Sediments - Evidence From Sr/Ca Ratios and Interstitial Dissolved Sr^{2+} Data, *J Sed Res*, *52*(1).

Bathurst, R. G. C. (1975), Carbonate sediments and their diagenesis, *Elsevier Science*.

Bé, A. W. H., and L. Lott (1964), Shell Growth and Structure of Planktonic Foraminifera, *Science*, *145*(3634), 823–824.

Berger, W. H. (1970), Planktonic Foraminifera: Selective solution and the lysocline, *Mar Geol*, *8*, 111–138.

Berger, W. H., M. C. Bonneau, and F. L. Parker (1982), Foraminifera on the deep-sea floor-lysocline and dissolution rate, *Oceanologica Acta*, *5*, 249–258.

Berner, R. A. (1980), Early Diagenesis: A Theoretical Approach, *Princeton University Press*.

Berner, R. A., and J. W. Morse (1974), Dissolution kinetics of calcium carbonate in sea water; IV, Theory of calcite dissolution, *274*(2), 108–134.

Brown, S., and H. Elderfield (1996), Variations in Mg/Ca and Sr/Ca ratios of planktonic foraminifera caused by postdepositional dissolution: Evidence of shallow Mg-dependent dissolution, *Paleoceanography*, *11*, 543–551.

Caron, D. A., O. R. Anderson, J. L. Lindsey, and W. W. Faber (1990), Effects of gametogenesis on test structure and dissolution of some spinose planktonic foraminifera and implications for test preservation, *Marine Micropaleontology*, *16*, 93–116.

de Deckker, P. (2004), On the celestite-secreting Acantharia and their effect on seawater strontium to calcium ratios, *Hydrobiologia*, *517*(1-3), 1–13.

de Nooijer, L. J., H. J. Spero, J. Erez, J. Bijma, and G.-J. Reichart (2014), Biomineralization in foraminifera, *Earth Science Reviews*, *135*, 48–58.

Dodd, J. (1967), Magnesium and strontium in calcareous skeletons: a review, *J Paleontol*, *41*, 1313–1329.

Edgar, K. M., E. Anagnostou, P. N. Pearson, and G. L. Foster (2015), Assessing the impact of diagenesis on δ11B, δ13C, δ18O, Sr/Ca and B/Ca values in fossil planktic foraminiferal calcite, *Geochim Cosmochim Ac*, *166*(C), 189–209.

Elderfield, H., J. M. Gieskes, P. A. Baker, R. K. Oldfield, C. J. Hawkesworth, and R. Miller (1982), $^{87}Sr/^{86}Sr$ and $^{18}O/^{16}O$ ratios, interstitial water chemistry and diagenesis in deep-sea carbonate sediments of the Ontong Java Plateau, *Geochim Cosmochim Ac*, *46*, 2259–2268.

Elderfield, H., J. Yu, P. Anand, T. Kiefer, and B. Nyland (2006), Calibrations for benthic foraminiferal Mg/Ca paleothermometry and the carbonate ion hypothesis, *EPSL*, *250*, 633–649.

Fantle, M. S., and D. J. DePaolo (2006), Sr isotopes and pore fluid chemistry in carbonate sediment of the Ontong Java Plateau: Calcite recrystallization rates and evidence for a rapid rise in seawater Mg over the last 10 million years, *Geochim Cosmochim Ac*, *70*(15), 3883–3904.

Fehrenbacher, J. S., and P. A. Martin (2014), Exploring the dissolution effect on the intrashell Mg/Ca variability of the planktic foraminifer Globigerinoides ruber, *Paleo-*

ceanography, *29*(9), 854–868.

Folk, R. L. (1965), Some Aspects of Recystallization in Ancient Limestones, *Dolomitization and Limestone Diagenesis*, *13*, 14–48.

Frank, T. D., M. A. Arthur, and W. E. Dean (1999), Diagenesis of Lower Cretaceous pelagic carbonates, North Atlantic: Paleoceanographic signals obscured, *J Foram Res*, *29*, 340–351.

Friedman, G. M. (1964), Early Diagenesis and Lithification in Carbonate Sediments, *J Sed Res*, *Vol. 34*.

Hales, B. (2003), Respiration, dissolution, and the lysocline, *Paleoceanography*.

Hathorne, E. C., O. Alard, R. H. James, and N. W. Rogers (2003), Determination of intratest variability of trace elements in foraminifera by laser ablation inductively coupled plasma-mass spectrometry, *Geochem. Geophys. Geosyst.*, *4*(12), n/a–n/a.

Helsel, D. R. (1990), Less than obvious - statistical treatment of data below the detection limit, *Env Sci Tech*, *24*(12), 1766–1774.

Hemleben, C. (1975), Spine and pustule relationships in some recent planktonic foraminifera, *Micropaleontology*.

Hemleben, C., M. Spindler, and O. R. Anderson (1989), *Modern Planktonic Foraminifera*, Springer-Verlag.

Hill, T. M., M. LaVigne, H. Spero, T. Guilderson, B. Gaylord, and D. Clague (2012), Variations in seawater Sr/Ca recorded in deep-sea bamboo corals, *Paleoceanography*, *27*(3), PA3202.

Honjo, S., and J. Erez (1978), Dissolution rates of calcium carbonate in the deep ocean; an in-situ experiment in the North Atlantic Ocean, *EPSL*, *40*(2), 287–300.

Johnstone, H. J. H., M. Schulz, S. Barker, and H. Elderfield (2010), Inside story: An X-ray computed tomography method for assessing dissolution in the tests of planktonic foraminifera, *77*(1-2), 58–70.

Johnstone, H. J. H., J. Yu, H. Elderfield, and M. Schulz (2011), Improving temperature estimates derived from Mg/Ca of planktonic foraminifera using X-ray computed tomography–based dissolution index, XDX, *Paleoceanography*, *26*(1).

Jones, E., T. Oliphant, P. Peterson, et al. (2001), SciPy: Open source scientific tools for Python, [Online; accessed 2015-06-20].

Kozdon, R., T. Ushikubo, N. T. Kita, M. Spicuzza, and J. W. Valley (2009), Intratest oxygen isotope variability in the planktonic foraminifer N. pachyderma: Real vs. apparent vital effects by ion microprobe, *Chem Geol*, *258*(3-4), 327–337.

Kozdon, R., D. C. Kelly, N. T. Kita, J. H. Fournelle, and J. W. Valley (2011), Planktonic foraminiferal oxygen isotope analysis by ion microprobe technique suggests warm tropical sea surface temperatures during the Early Paleogene, *Paleoceanography*, *26*(3), PA3206–n/a.

Kozdon, R., D. C. Kelly, K. Kitajima, and A. Strickland (2013), In situ δ18O and Mg/Ca analyses of diagenetic and planktic foraminiferal calcite preserved in a deep-sea record of the Paleocene-Eocene thermal maximum, *Paleoceanography*, *28*, 517–528.

Lingen, G. J. v. d., and G. h. Packham (1975), Relationships between diagenesis and physical properties of biogenic sediments of the Ontong-Java plateau (Sites 288 and

289, Deep Sea Drilling Project), *deepseadrilling.org*.

Lohmann, G. P. (1995), A model for variation in the chemistry of planktonic foraminifera due to secondary calcification and selective dissolution, *Paleoceanography*, *10*, 445–457.

Lorens, R., D. Williams, and M. L. Bender (1977), The Early Nonstructural Chemical Diagenesis of Foraminiferal Calcite, *J Sed Res*, *47*, 1602–1609.

Mavromatis, V., Q. Gautier, O. Bosc, and J. Schott (2013), Kinetics of Mg partition and Mg stable isotope fractionation during its incorporation in calcite, *Geochimica et Cosmochimica ....*

McCorkle, D. C., P. A. Martin, D. W. Lea, and G. P. Klinkhammer (1995), Evidence of a dissolution effect on benthic foraminiferal shell chemistry: $\delta^{13}C$, Cd/Ca, Ba/Ca, and Sr/Ca results from the Ontong Java Plateau, *Paleoceanography*, *10*, 699–714.

Mekik, F., and L. Raterink (2008), Effects of surface ocean conditions on deep-sea calcite dissolution proxies in the tropical Pacific, *Paleoceanography*, *23*(1).

Milliman, J. D., P. J. Troy, W. M. Balch, A. K. Adams, Y. H. Li, and F. T. Mackenzie (1999), Biologically mediated dissolution of calcium carbonate above the chemical lysocline?, *Deep Sea Res Pt I*, *46*(10), 1653–1669.

Morse, J. W., and R. S. Arvidson (2002), The dissolution kinetics of major sedimentary carbonate minerals, *58*(1-2), 51–84.

Morse, J. W., R. S. Arvidson, and A. Luttge (2007), Calcium carbonate formation and dissolution, *Chem Rev*, *107*(2), 342–381.

Mucci, A. (1987), Influence of temperature on the composition of magnesian calcite overgrowths precipitated from seawater, *Geochim Cosmochim Ac*, *51*(7), 1977–1984.

Mucci, A., and W. Morse (1983), The incorporation of Mg^{2+} and Sr^{2+} into calcite overgrowths: influences of growth rate and solution composition, *Geochim Cosmochim Ac*.

Nehrke, G., G. J. Reichart, P. van Cappellen, C. MEILE, and J. Bijma (2007), Dependence of calcite growth rate and Sr partitioning on solution stoichiometry: Non-Kossel crystal growth, *Geochim Cosmochim Ac*, *71*(9), 2240–2249.

Oomori, T., H. Kaneshima, Y. Maezato, and Y. Kitano (1987), Distribution Coefficient of Mg^{2+} Ions Between Calcite and Solution at 10-50-Degrees-C, *Mar Chem*, *20*(4), 327–336.

Orr, W. N. (1967), Secondary Calcification in the Foraminiferal Genus Globorotalia, *Science*, *157*(3796), 1554–1555.

Pearson, P., P. Ditchfield, and J. Singano (2001), Warm tropical sea surface temperatures in the Late Cretaceous and Eocene epochs, *Nature*, *413*, 401–407.

Pearson, P. N., and C. E. Burgess (2008), Foraminifer test preservation and diagenesis: comparison of high latitude Eocene sites, *Geol Soc, Lon, Spec Pub*, *303*(1), 59–72.

Pešić, Z. D., A. D. Fanis, U. Wagner, and C. Rau (2013), Experimental stations at I13 beamline at Diamond Light Source, *J Phys: Conf Series*, *425*.

Rau, C., V. Crecea, W. Liu, C. P. Richter, K. M. Peterson, P. R. Jemian, U. Neuhäusler, G. Schneider, X. Yu, P. V. Braun, T. C. Chiang, and I. K. Robinson (2007a), Synchrotron-based imaging and tomography with hard X-rays, *Nuc Inst Meth Phys Res B*, *261*, 850–854.

Rau, C., V. Crecea, C. P. Richter, K. M. Peterson, P. R. Jemian, U. Neuhäusler, G. Schneider, X. Yu, P. V. Braun, T. C. Chiang, and I. K. Robinson (2007b), Imaging of micro- and nano-structures with hard X-rays, *Micro Nano Lett*, *2*, 1–5.

Rau, C., U. Wagner, Z. D. Pešić, and A. D. Fanis (2011), Coherent Imaging at the Diamond Beamline I131, *Phys Status Solidi A*, *208*, 2522–2525.

Regenberg, M., D. Nürnberg, S. Steph, J. Groeneveld, D. Garbe-Schonberg, R. Tiedemann, and W.-C. Dullo (2006), Assessing the effect of dissolution on planktonic foraminiferal Mg/Ca ratios: Evidence from Caribbean core tops, *Geochem. Geophys. Geosyst.*, *7*(7).

Regenberg, M., A. Regenberg, D. Garbe-Schonberg, and D. W. Lea (2014), Global dissolution effects on planktonic foraminiferal Mg/Ca ratios controlled by the calcite-saturation state of bottom waters, *Paleoceanography*, *29*(3), 127–142.

Richter, F. M., and D. J. DePaolo (1987), Numerical-Models for Diagenesis and the Neogene Sr Isotopic Evolution of Seawater From DSDP Site 590B, *EPSL*, *83*, 27–38.

Richter, F. M., and D. J. DePaolo (1988), Diagenesis and Sr isotopic evolution of seawater using data from DSDP 590B and 575, *EPSL*, *90*, 382–394.

Richter, F. M., and Y. Liang (1993), The rate and consequences of Sr diagenesis in deep-sea carbonates, *EPSL*, *117*, 553–565.

Rosenthal, Y., and E. A. Boyle (1993), Factors controlling the fluoride content of planktonic foraminifera: An evaluation of its paleoceanographic applicability, *Geochim Cosmochim Ac*, *57*, 335–346.

Rosenthal, Y., G. P. Lohmann, K. C. Lohmann, and R. M. Sherrell (2000), Incorporation and preservation of Mg in Globigerinoides sacculifer: implications for reconstructing the temperature and 18O/16O of seawater, *Paleoceanography*, *15*(1), 135–145.

Ruiz-Agudo, E., C. V. Putnis, C. Rodriguez-Navarro, and A. Putnis (2012), Mechanism of leached layer formation during chemical weathering of silicate minerals, *Geology*, *40*(10), 947–950.

Russell, A. D. (1994), Uranium in foraminiferal calcite: Incorporation, preservation and seawater record, *PhD Thesis, University of Washington, Seattle*.

Sadekov, A. Y., S. M. Eggins, and P. de Deckker (2005), Characterization of Mg/Ca distributions in planktonic foraminifera species by electron microprobe mapping, *Geochem Geophys Geosyst*, *6*.

Sadekov, A. Y., S. Eggins, G. P. Klinkhammer, and Y. Rosenthal (2010), Effects of seafloor and laboratory dissolution on the Mg/Ca composition of Globigerinoides sacculifer and Orbulina universa tests - A laser ablation ICPMS microanalysis perspective, *EPSL*, *292*(3-4), 312–324.

Savin, S. M., and R. G. Douglas (1973), Stable Isotope and Magnesium Geochemistry of Recent Planktonic Foraminifera from the South Pacific, *Geol Soc Am Bull*, *84*, 2327–2342.

Schindelin, J., I. Arganda-Carreras, E. Frise, V. Kaynig, M. Longair, T. Pietzsch, S. Preibisch, C. Rueden, S. Saalfeld, B. Schmid, J.-Y. Tinevez, D. J. White, V. Hartenstein, K. Eliceiri, P. Tomancak, and A. Cardona (2012), Fiji: an open-source platform for biological-image analysis., *Nat Methods*, *9*, 676–682.

607 Schmidt, D. N., E. J. Rayfield, A. Cocking, and F. Marone (2013), Linking evolution
608 and development: Synchrotron Radiation X-ray tomographic microscopy of planktic
609 foraminifers, *Palaeontology*, *56*(4), 741–749.

610 Schrag, D., D. J. DePaolo, and F. M. Richter (1995), Reconstructing Past Sea-Surface
611 Temperatures - Correcting for Diagenesis of Bulk Marine Carbonate, *Geochim Cos-*
612 *mochim Ac*, *59*, 2265–2278.

613 Schrag, D. P. (1999), Effects of diagenesis on the isotopic record of late paleogene tropical
614 sea surface temperatures, *Chem Geol*, *161*, 215–224.

615 Sexton, P. F., P. A. Wilson, and P. N. Pearson (2006), Microstructural and geochem-
616 ical perspectives on planktic foraminiferal preservation: "Glassy" versus "Frosty",
617 *Geochem Geophys Geosyst*, *7*.

618 Shipboard Scientific Party (2001), Leg 192 Preliminary Report: Basement drilling of
619 the Ontong Java Plateau, *ODP Prelim Rpt*, *92*.

620 Wolf, K. B., and G. Krötzsch (1995), Geometry and dynamics in refracting systems,
621 *Eur J Phys*, *16*, 14–20.

622 Yushkevich, P. A., J. Piven, H. C. Hazlett, R. G. Smith, S. Ho, J. C. Gee, and G. Gerig
623 (2006), User-guided 3D active contour segmentation of anatomical structures: signif-
624 icantly improved efficiency and reliability, *Neuroimage*, *31*, 1116–1128.

Table 1. The different types of calcite described in foraminifera. Adapted from *Hemleben et al.* [1989].

Calcite Type	Description
Primary/Chamber	Calcite formed during the prolocular or juvenile stages of the foraminiferal life cycle. Typically porous, with pronounced laminations separated by organic- and Mg-rich layers. Forms a base for the spines, in spinose species.
Keel	An angled rim surrounding the outer edge foraminifera with reinforcing elements. A build up of calcite around the edges of the test often leads to a bulbous rim to the test, which is structurally distinct from chamber calcite. The primary difference is the lack of pores in the calcite, although laminations are still present.
Gametogenic	A thick encrusting layer of calcite, formed in the latter stages of the foraminiferal life cycle, often prior to the release of gametes during sexual reproduction (hence 'gametogenic').
Crust	Any crust deposited over the whole of the original test structure. Gametogenic crusts can often be considered under this umbrella term, but crusts can also include MnO crusts, or calcite precipitated during diagenesis. In general, the origin and nature of foraminiferal 'crusts' are poorly understood, and diverse.

Figure 1. A representative tomogram (top) and 2D image slice (bottom) of *G. tumida* specimens from the seven depth sites considered. Note the transition from a well-formed, 'pristine' ultrastructure in the shallowest specimen, to a blocky encrusted appearence in the deepest specimen. The deeper specimen also lacks any internal test structure. The top two rows of samples are from above the lysocline ($\sim$ 3400 m), and the bottom row are from below. Numbers above the tomograms indicate coretop water depth. See supplementary images for further tomograms and image slices of all specimens.

Figure 2. Tomographic slices through shallow (left) and deep (right) foraminiferal specimens, showing the 'pristine' state (left), with chamber (red) and keel (yellow) calcite highlighted, and the 'modified' state (right), with chamber (red), keel (yellow) and crust (blue) calcites, as defined in Table 1. For the purposes of segmentation, the keel and chamber calcite types are considered together as 'chamber' calcite. Pristine chamber calcite in shallow specimens exhibits internal laminations and fine pore structures, while in deep specimens the chamber calcite visibly deteriorates, with internal dissolution along the laminations. The crust calcite lacks internal laminations, and pores are less regular or absent. These features are evident throughout the specimens in Figure 1.

Figure 3. The change in length-normalised test thickness, crust abundance and chamber calcite abundance with core top depth. All data are normalised to maximum external test length. In the abundance plots, black triangles indicate 3D data segmentation, while coloured dots represent segmented 2D slices. The grey background denotes sub-lysocline depths. There is a marked linear increase in test thickness with core top depth. There is also a trend for increased crust abundance, and decreased chamber calcite abundance with depth. These trends are seen in both 2D and 3D data, although the scatter in the 2D data is large, reflecting the variability of alteration throughout the test.

Figure 4. The change in the relative abundance (%) of chamber (solid red, solid line) and crust (hollow blue, dashed line) calcite within the test with depth, calculated by an end-member mixing model [*Brown and Elderfield*, 1996] and directly measured from 3D tomographic data (this study). Each technique yields a similar trend of more chamber calcite in shallow water, and more crust in deep water, but the magnitude of the trends vary significantly. These data represent a change in the *relative abundance* of the materials, which could represent either a dissolution of test or a precipitation of crust, or a combination of the two.

Figure 5. The Mg/Ca (left) and Sr/Ca (right) of chamber (red) and crust (blue) calcite in all analyses (top, histogram), and with depth (bottom). Chamber calcite has significantly higher Mg/Ca and Sr/Ca than crust calcite. The Mg/Ca and Sr/Ca of crust and whole-test calcite decreased significantly with depth, while chamber calcite did not. See methods section for statistics. Lines are the median, and error envelope is the inter-quartile range of the data.

1614 m

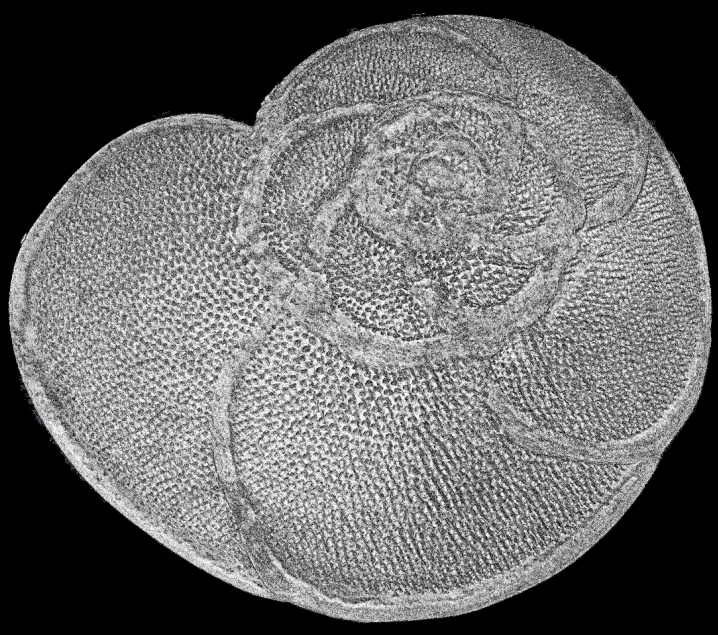

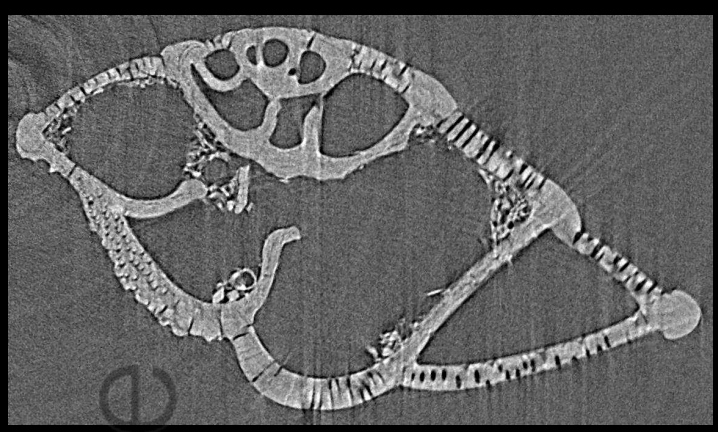

2016 m

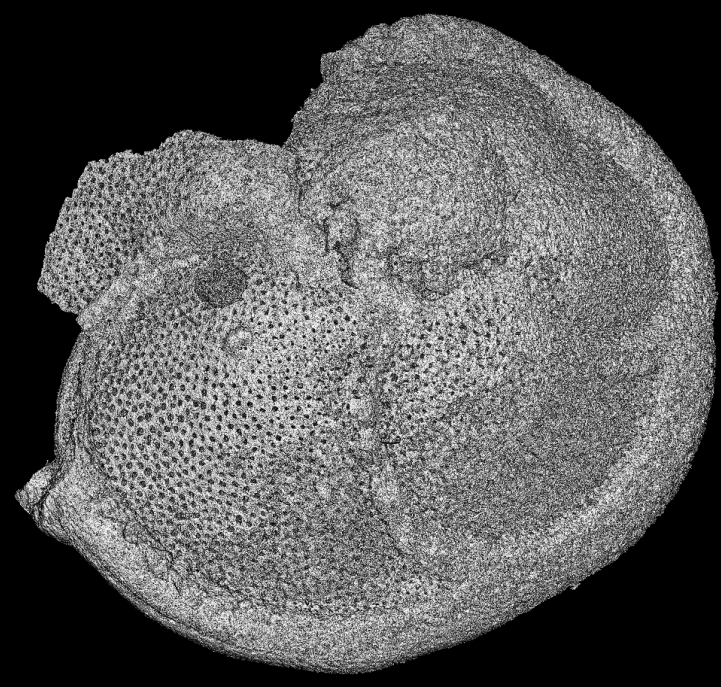

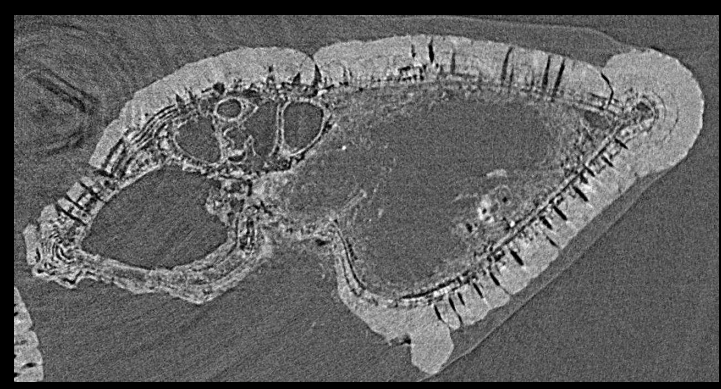

2445 m

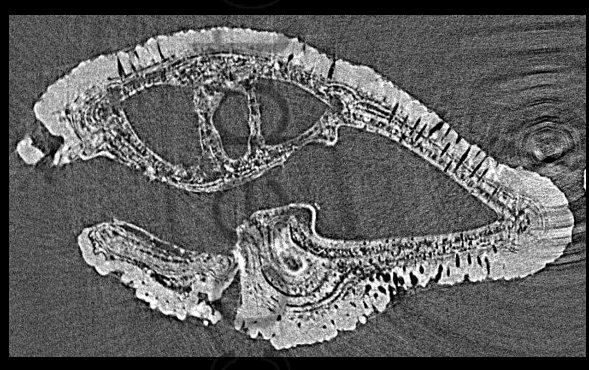

2959 m

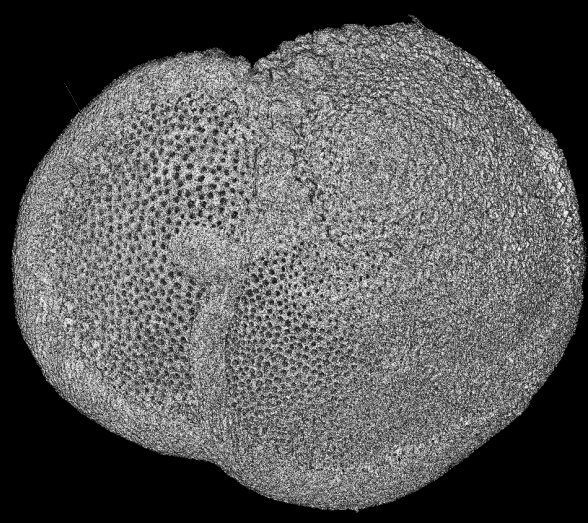

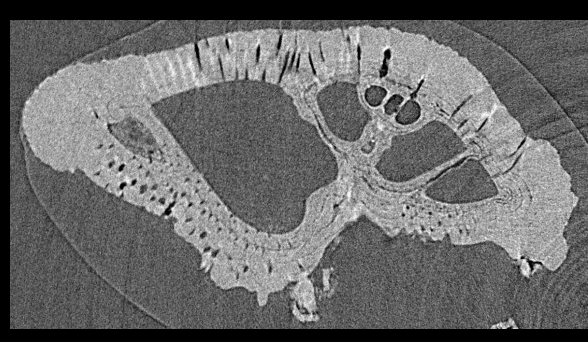

3411 m

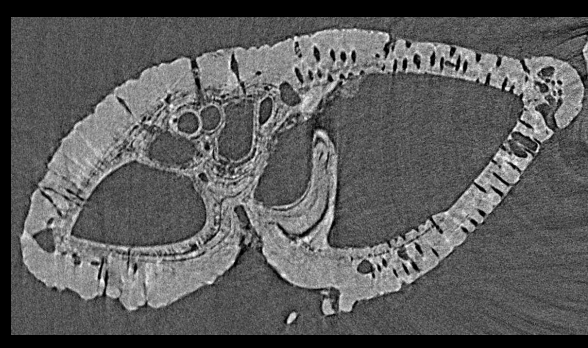

4025 m

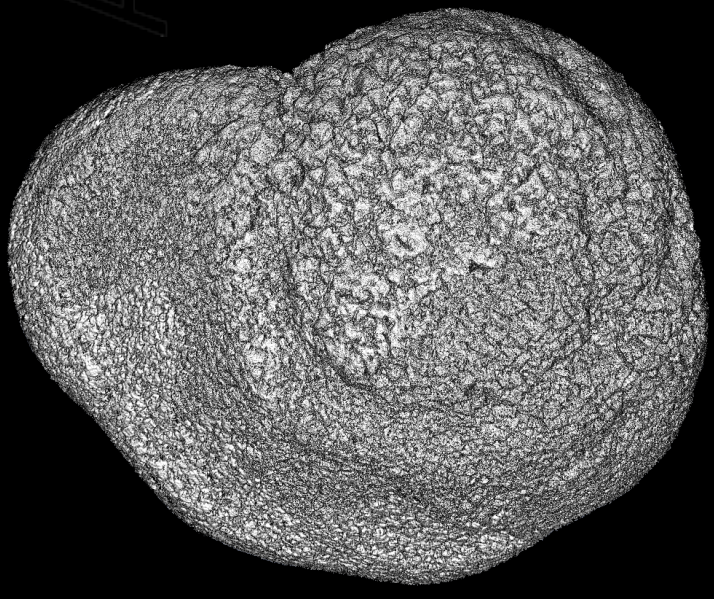

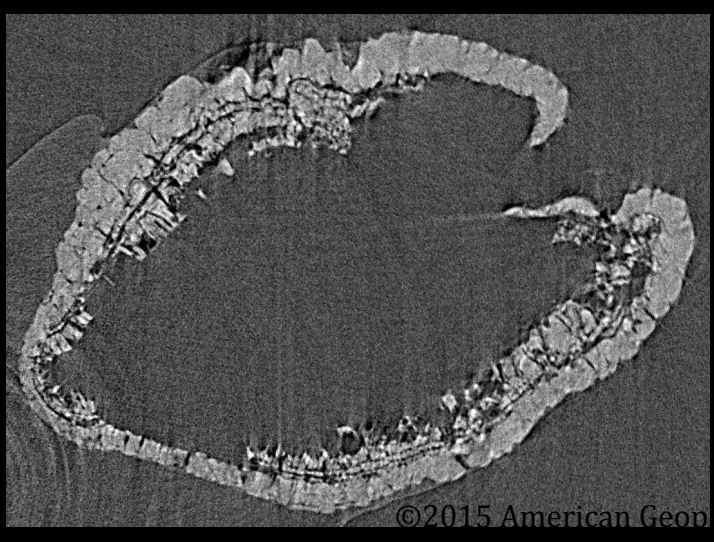

4341 m